DEVELOPMENT OF IMPROVED DESIGN PROCEDURES FOR NEAR FAULT GROUND MOTIONS

H. Krawinkler and B. Alavi

Department of Civil and Environmental Engineering
Stanford University

ABSTRACT

The results of the study summarized here are intended to shed light on some of the important issues that affect the response of structures to near fault ground motions. Attempts are presented to identify salient response characteristics, to describe near fault ground motions by properties of equivalent pulses, and to utilize the pulse response characteristics to define behavior attributes of structures when subjected to near fault ground motions. The ultimate objective is to develop improved design procedures. Preliminary recommendations are made in this respect, but it must be understood that much more work needs to be done before comprehensive answers will be found.

INTRODUCTION

Recordings from recent earthquakes have provided much evidence that ground shaking near a fault rupture is characterized by a small number of pulses (often only one) with very high energy input. This holds true particularly in the "forward" direction, where the propagation of the fault rupture towards a site at a velocity close to the shear wave velocity causes most of the seismic energy from the rupture to arrive in a single large long-period pulse of motion that occurs at the beginning of the record (Somerville et al., 1997). The radiation pattern of the shear dislocation on the fault causes this large pulse of motion to be oriented in the direction perpendicular to the fault, causing the strike-normal peak velocity to be larger than the strike-parallel peak velocity (Somerville, 1998). This phenomenon requires consideration in the design process for structures that are located in the "near-fault" region, which is usually assumed to extend 10 to 15 km from the seismic source (1996 SEAOC Bluebook). Recent guidelines and codes have recognized the existence of the problem by providing magnitude and distance dependent "near source factors" that are applied directly to the design spectrum (or base shear) values.

The near source factors recommended presently may be considered as a stopgap measure that gives recognition to the problem but does not necessarily provide a final answer. The measure of increasing the design base shear without modifying the design shear force distribution over the height of the structure may not solve the problem. Moreover, the recent emphasis on performance-based seismic design makes it necessary to explicitly assess performance at different levels, ranging from immediate occupancy to collapse prevention, i.e., from nearly elastic behavior to near-collapse behavior. Much research is needed to identify and quantify the magnitude and distance dependent characteristics of near fault ground motions and address all the issues concerned with the response of different types of structures subjected to different types of near fault ground motions. This paper addresses only small parts of a big

problem, but the authors hope that the presented ideas and concepts will help in forming a foundation on which to base further research and development and, ultimately, a design procedure that will provide adequate and consistent protection of structures and their contents in near fault regions.

The results of the study summarized here are intended to shed light on some of the important issues that affect the response of structures to near fault ground motions. Attempts are presented to identify salient response characteristics, to describe near fault ground motions by properties of equivalent pulses, and to utilize the pulse response characteristics to define behavior attributes of structures when subjected to near fault ground motions. The ultimate objective is to develop improved design procedures. Preliminary recommendations are made in this respect, but it must be understood that much more work needs to be done before comprehensive answers will be found.

The conclusions drawn later have to be interpreted in the context of the assumptions that had to be made in order to arrive at preliminary answers to a complex problem. Some of the assumptions are summarized here:

- It is assumed that the two sets of near fault records used in this study cover the range of characteristics contained in typical near fault ground motions.
- Only ground motions in soil (NEHRP soil type D) are considered.
- Only the worst-case scenario is investigated; i.e., only forward directivity is considered, and the response evaluation is performed for the fault-normal component of the ground motion.
- This study is concerned only with the response of two-dimensional generic frames whose design and response behavior follow certain patterns that are described later.
- It is assumed that inelastic seismic response is controlled by the shear strength provided in each story, and that the story ductility ratio is the basic performance parameter.
- The emphasis is on long period frame structures whose fundamental period is longer than the period of the pulse that characterizes the near fault ground motion.
- Structures whose response is controlled by overturning moments (such as most wall-type structures) are not considered.

NEAR FAULT GROUND MOTION RECORDS USED IN THIS STUDY

The records used in this study are discussed in more detail in Somerville (1998). Recorded and simulated motions are available for dynamic analysis. The designation and basic properties of the recorded soil motions are listed in Table 1. These motions cover a magnitude range from 6.2 to 7.4 and a distance range from 0.0 to 10.0 km, without a systematic pattern. The simulated motions represent two stations (f6 and f8) and cover systematic ranges of magnitude (6.5, 7.0, and 7.5) and distance (3, 5, and 10 km). For the analytical study summarized in this paper, only the fault-normal components of soil records with forward directivity are utilized. A total of 15 recorded motions and 18 simulated motions are available for this purpose.

Typical acceleration (elastic strength demand), velocity, and displacement spectra for two recorded time history pairs (both the fault-normal and fault-parallel components of a record) are presented in Fig. 1. The figure shows clearly the large difference between the fault-normal and fault-parallel components, and indicates in the velocity spectra a dominant peak at a well defined period (at 1.0 sec. for LP89lex, and 2.4 sec. for NR94sylm). As will be shown later, this period can be designated as the period of an equivalent pulse. Typical spectra for simulated ground motions are presented in Fig. 2. A predominant period is again evident in the velocity spectra. The figure illustrates the magnitude and distance dependence of the spectra.

A reference set of 15 "standard" records is utilized for comparison purposes. These records were used in past studies (Seneviratna and Krawinkler (1997) and are scaled in a manner so that the spectrum of each individual record matches the NEHRP soil type D spectrum with a minimum error, using discrete periods in the range of 0.6 to 4.0 seconds (constant velocity range). The mean acceleration spectrum of the 15 scaled records, referred to as 15-D* (mean), is shown in Fig. 3 together with the NEHRP soil type D spectrum. Thus, in average, these 15-D* time histories are reasonable representations of presently employed design ground motions.

Figure 4 shows the mean velocity spectrum of the 15-D* records superimposed on the velocity spectra of several of the recorded near fault time histories. This figure is presented for two reasons. First, to illustrate the great variability in the response spectra that have to be expected from near fault ground motions, and second, to put the severity of near fault ground motions in perspective with present design ground motions. Maximum values of spectral velocities of the near fault records are several times those of the means of the design ground motions. Even though this figure presents an unduly negative picture (only fault-normal components of the near fault records are used, and individual records of the 15-D* set have also relatively large peaks), it points out that near fault records can impose very large demands that need to be considered in the design process. The response of structures to the ground motions represented by these spectra is discussed later.

SDOF AND MDOF SYSTEMS USED IN THIS STUDY

In the dynamic studies the structural systems are assumed to have 2% damping ($\xi = 2\%$) rather than the customary 5%. The reason is that long period flexible structures are often steel frame structures for which 5% damping is difficult to justify. For SDOF response studies bilinear nondegrading load-deformation characteristics are used, usually with 3% strain hardening ($\alpha = 3\%$).

MDOF structural systems are represented by a generic 2-dimensional single-bay frame whose strength and stiffness properties are tuned to specific requirements. The fundamental elastic period T is considered as a variable, but the number of stories is kept constant at 20. Story masses and story heights are assumed uniform over the height of the structure. The beam and column stiffnesses are tuned such that a straight line deflected shape results under a shear force pattern that corresponds to the SRSS combination of modal shear forces under a 1/T–type response spectrum. For strength design the same SRSS shear force pattern is used to tune the member bending strengths in a manner that results in simultaneous yielding at all plastic hinge locations. Inelastic deformations are permitted only at plastic hinge locations at the column base and at beam ends, resulting in a mechanism that involves the full structure, see Fig. 5. In this

manner structures are generated whose story shear strengths are tuned to the widely used SRSS load pattern for a standard design spectrum. The base shear that causes yielding in the structure is denoted as V_y, and the lateral strength of the structure is defined in a dimensionless form by the parameter $\gamma = V_y / W$.

At all plastic hinge locations a bilinear nondegrading moment-rotation model with 3% strain hardening is used. This member hardening rule results in a story hardening stiffness of 3.6% for structures in which P-delta effects are neglected. Designs with P-delta effects are also performed. In these designs the magnitude of the gravity loads is tuned such that the elastic second order effect in the first story amounts to 10% (in present codes such a second order effect does not require design modifications). This P-delta effect results in a negative story stiffness of –2.8% of the elastic stiffness in the first story of the structure. The lateral load (base shear) vs. first story drift relationships with and without P-delta effect, obtained from a pushover analysis, are shown in Fig. 6. Even though the negative stiffness is rather small, the effects of P-delta were found to vary from negligible to dominant, depending on the case studied. This paper focuses only on behavior of structures without P-delta effects. However, it must be emphasized that the results of this study have demonstrated that P-delta effects may have a dominant effect on structural response and, in general, deserve serious consideration.

RESPONSE OF SDOF AND MDOF SYSTEMS TO PULSE INPUT

In order to acquire a basic understanding of the response of structures to pulse loading of the type represented by near fault ground motions, elastic and inelastic dynamic analyses are performed on SDOF and MDOF systems using pulses as input motions. Various pulses are investigated, with the most basic ones being denoted as half pulse (P1), full pulse (P2) and multiple pulse (P3). The acceleration, velocity, and displacement time histories of pulses P2 and P3 are shown in Fig. 7. Pulse P1 consists of half of pulse P2. The pulses are fully defined by the pulse period T_p and the peak ground acceleration $a_{g,max}$. Other pulses with linear acceleration wave forms and with different configurations have also been studied, but it was found that their response characteristics do not differ by much from those of the three basic pulses.

Elastic spectral properties of the three basic pulses are presented in Fig. 8. The period axis is normalized to the pulse period T_p and the spectral values are normalized to the peak time history values. Peaks in the velocity spectra at $T/T_p = 1.0$ are clearly evident for pulses P2 and P3. In the interpretation it must be considered that the peak displacement $u_{g,max}$ of Pulse P3 is only half the value of the peak displacement of Pulses P1 and P2 (this explains the very large normalized spectral displacement values for P3). The inelastic strength demand spectra for specific ductility values, presented in Fig. 9, show large fluctuations for T/T_p values smaller than 1.0 but consistent and well established patterns (e.g., large strength reduction factors at the periods at which the elastic spectra have a peak) for T/T_p values of 1.0 or larger.

Story shear demand patterns over the height of the structure for elastic MDOF systems with various T/T_p ratios subjected to pulse P3 are shown in Fig. 10. Results are obtained from time history analysis (Fig. 10(a)) and SRSS modal combinations obtained from the pulse spectrum (Fig. 10(b)). Shown on both figures is also the SRSS pattern from the 1/T-type spectrum that is used for strength design. The important observations are that for T/T_p values greater than 1.0 the shear force patterns exhibit a traveling wave effect that results in very high

story shears in upper stories, and that the SRSS modal combination is not a good surrogate for dynamic story shear forces, particularly if $T/T_p > 1.0$. This observation provides a hint that spectral analysis may not capture all important response characteristics of structures subjected to pulse-type ground motions. This is likely true for structures responding elastically and certainly true for structures responding inelastically.

The inelastic response of MDOF systems to pulse-type inputs shows special and peculiar characteristics, which later will be confirmed also for the response to near fault ground motions. The inelastic response is described here by maximum story ductility ratios, μ_i, which become greater than 1.0 when the shear strength in any story is smaller than that causing elastic response. The base shear strength of MDOF systems subjected to pulse-type inputs is defined by the ratio $\eta = V_y/ma_{g,max}$. Distributions of ductility demands over the height of the structure for pulses P2 and P3 and ratios of $T/T_p = 1.0$ and 2.0 are shown in Figs. 11 and 12 for various η values.

Since the MDOF structures are designed for a story shear force pattern corresponding to the SRSS modal combination for a 1/T-type spectrum ("SRSS Pattern" in Fig. 10), it is expected that yielding will start in those stories in which the elastic story shear demand pattern exceeds the "SRSS Pattern" by the largest amount. As Fig. 10(a) indicates, for pulse P3 and $T/T_p = 2.0$ this occurs about 2/3rd up the height of the structure. Figure 12(a) shows that the ductility demands are highest at this location, for relatively strong structures (large η values). However, for weak structures (small η values) a clear migration occurs of maximum ductility demands to the bottom of the structure. At the 2/3rd level the ductility demands stabilize around 3 and grow no further, whereas at the lower stories the ductility demands increase rapidly. The same phenomenon is observed for pulse P2 and $T/T_p = 2.0$ (Fig. 11(a)).

The consistency of this phenomenon is surprising and deserves much scrutiny because it is one of the basic phenomena of pulse-type and near fault ground motion response. Clearly it has to do with the traveling wave effect that occurs primarily for $T/T_p > 1.0$. At $T/T_p = 1.0$ this phenomenon starts to occur but is not yet very pronounced (see Figs. 11(b) and 12(b)).

A comprehensive picture of the maximum story ductility demand for pulse-type input, regardless of location in the structure, can be obtained from the $\eta - \mu_{max}$ diagrams presented for various T/T_p ratios in Figs. 13 and 14. Figure 13, which is for pulse P2, shows a distinct stabilization range at a maximum ductility ratio of about 3 for T/T_p values larger than 1.0. In this range the base shear strength can be reduced by a factor larger than 2 without causing much, if any, increase in ductility demand. However, once a threshold of strength is reached, the ductility demand increases rapidly for a small reduction in strength. This is the threshold when the critical story has migrated from the upper portion to the bottom of the structure.

The strong statement made about stabilization of ductility demands has to be put in perspective. The results presented here are obtained for structures whose relative story shear strength follows the SRSS shear force distribution for a 1/T-type design spectrum. Thus, the results are useful for performance evaluation of structures designed according to present practice. This is not to say that a strength design according to this shear force distribution is desirable. Desirable shear strength distributions are discussed later. Also, the results presented here for pulse-type inputs are relevant only if actual near fault ground motions can be represented by equivalent pulses. This issue is also discussed later.

RESPONSE OF MDOF SYSTEMS TO NEAR FAULT GROUND MOTIONS

The fundamental observations made on response characteristics of MDOF systems to pulse inputs apply also to near fault ground motions. For elastic systems a traveling wave effect for long-period structures is evident in the story shear distribution over the height. This traveling wave effect is partially but not fully captured by an SRSS modal analysis; see Figure 15, which can be compared to Fig. 10. This wave effect has similar consequences on the inelastic response as were discussed for pulse inputs.

Figure 16 shows the distribution of story ductility demands over the height of the structure for the near fault records whose velocity spectra are shown in Fig. 4, for MDOF systems with a fundamental period T = 2.0 sec. and a base shear strength defined by $\gamma = V_y/W = 0.15$. For records for which the ductility demands are small the demands are about the same over the height, but for records for which the demands are large there is a concentration of demands near the base of the structure. In the upper story the ductility demands do not exceed a value of about 5. Thus, a migration of demands towards the base is evident as the ground motion becomes more severe (or the structure becomes weaker). For comparison, the mean story ductility demands for the reference set of 15-D* records are also shown. The graph indicates that, in the mean, an SRSS based strength design results in a uniform ductility distribution – for standard ground motions. However, the same design results in great variations of ductility demands over the height when a structure is subjected to near fault ground motions.

A comprehensive assessment of maximum story ductility demands for the same records and MDOF systems with T = 2.0 sec. can be obtained from the $\gamma - \mu_{max}$ curves presented in Fig. 17. Many of the curves exhibit a kink (rapid change in slope) around a maximum ductility demand of about 3 to 4, which is the range in which the maximum story ductility demand migrates from the upper portion of the structure to the base. Again, a comparison of ductility demands between near fault records and the mean of the 15-D* records looks alarming, but it must be kept in mind that all near fault records are fault-normal components and that the curve for the 15-D* records shows only mean values but no peak values.

The story ductility migration phenomenon can be observed also in the story ductility demand graphs for individual records shown in Fig. 18. Distributions of demands over the height are shown for different γ values covering the range from elastic behavior to large ductility demands. In both cases the period is selected to be clearly larger than the period of the equivalent pulse (1.0 sec. for LP89lex and 2.4 sec. for NR94sylm). These results and others have demonstrated that important similarities exist between near fault responses and pulse responses. The issue of representing near fault records by equivalent pulses is pursued next.

REPRESENTATION OF NEAR FAULT GROUND MOTIONS BY EQUIVALENT PULSES

Figure 4 shows that near fault ground motions come in great variations. Any attempt to evaluate performance and/or develop design criteria would have to be extremely complex unless such ground motions can be represented by simplified motions that reasonably replicate the most important response characteristics of the near field motions. Based on (1) visual inspection of time history records, (2) inspection and evaluation of velocity and displacement response spectra,

and (3) evaluation of elastic and inelastic MDOF response characteristics it is concluded that within certain limitations near fault records can be represented by equivalent pulses of the type discussed previously.

It is unreasonable to expect that this equivalence can be established for the full period range of interest. In particular in the short period range the near fault time history trace is likely contaminated by many ancillary waves that have little to do with the characteristics of the long-period high-energy pulse generated by the propagation of fault rupture. It is also likely that in the very long period range other phenomena (e.g., basin effects) contaminate the record. But it is postulated that in the range of periods from about one to three times the pulse period an equivalence between a near fault ground motion and a pulse can be established with reasonable confidence. In the following discussion it is assumed that an equivalence can be established for the range of T/T_p from 0.75 to 3.0, where T is the fundamental period of the structure and T_p is the period of the equivalent pulse.

Much effort has been devoted to establishing such an equivalence through a consistent procedure. The writers do not claim that the issue has been resolved to full satisfaction. There are many successes, but not all near fault records used in this study have become part of this success. The present status is that promising results have been obtained, but it must be emphasized that many more records need to be evaluated and more work needs to be done before a full equivalence can be established with confidence.

Three parameters are needed to establish a record to pulse equivalence; the pulse type (P1, P2, or P3), the pulse period T_p, and the pulse severity. The peak acceleration of the square wave acceleration history, $a_{g,max}$, shown in Fig. 7 is used for the latter purpose. In the following discussion the $a_{g,max}$ of the equivalent pulse is referred to as the effective acceleration, a_{eff}. If these parameters are known, all other time history, spectral, and other response properties can be derived.

Engineering rather than seismological considerations are used in this study to deduce these parameters. Mostly judgment is employed to decide on the pulse type, based on an inspection of the time history trace and on a comparison between ground motion and pulse spectral shapes (primarily velocity and displacement spectra). A sensitivity study that supports these judgmental decisions still needs to be performed. The pulse period T_p is determined from the peaks of the velocity spectra. Typical examples are illustrated in Fig. 19, which shows the velocity spectra of the three basic pulses superimposed on the velocity spectra of two near fault records. In most cases a narrow range for T_p could be established rigorously, but at the end judgment had to be employed to decide on a final value.

Various procedures were investigated to determine the effective pulse acceleration a_{eff}; the simplest one being the estimation of a_{eff} from the elastic displacement spectra (equating pulse and ground motion spectral displacement at $T = T_p$). Inconsistent results were obtained when the so estimated values were used to compute ductility demands for MDOF systems. The reason is that no consideration is given to inelastic response characteristics when the determination of a_{eff} is based on elastic spectra only. Ultimately, a rigorous process was employed with the objective being the minimization of the differences between the maximum story ductility demands obtained from the near fault ground motion and the equivalent pulse. The following steps are used in this procedure:

1. Compute the η–μ_{max} curves for the selected pulse type for T/T_p = 0.75, 1.0, 1.5, 2.0, & 3.0.
2. Compute the γ–μ_{max} curves for the near fault record for T/T_p = 0.75, 1.0, 1.5, 2.0, and 3.0.
3. For each T/T_p value convert the η–μ_{max} curve of the pulse into a γ–μ_{max} curve [$\gamma = (a_{eff}/g)\eta$] and find best-fit values for a_{eff} by minimizing the relative differences between the two γ–μ_{max} curves for the following three ranges of μ_{max}: μ_{max} = 1 to 10 (full range of interest), μ_{max} = 4 to 10 (low performance levels), and μ_{max} = 1.0 (high performance level). The least-squares method is used to minimize the differences between the two curves.
4. Obtain final values for a_{eff} by averaging the best-fit values for the five period ratios. At this time this is done separately for the three ranges of μ_{max}.

The results of this procedure for the recorded and simulated near fault records are summarized in Tables 2 and 3, respectively. The tables list pulse type and period, as well as effective acceleration and peak velocity and displacement of the equivalent pulse for the three ductility ranges. The results are preliminary because a sensitivity study still needs to be performed. Even though the effective acceleration is used as the basic pulse parameter, the more relevant parameters for structural response evaluation are the peak velocity and displacement values (peak velocity = $a_{eff}T_p/4$).

The results for the simulated records are rather consistent and show clear patterns with magnitude and distance (for peak velocity and displacement, but not for a_{eff}). As expected, the values differ somewhat but not by a large amount between the three ductility ranges. Patterns for the recorded motions are not that evident, which may not be surprising when it is considered that these records come from several different events. The Landers (Lucerne) record (LN92lucr) has been omitted from Table 2 because it has a pulse period of greater than 4 seconds, which eliminates this record from consideration.

Figure 20 illustrates examples of "best" matches between the converted pulse γ–μ_{max} curves and the γ–μ_{max} curves for two ground motions, using the full ductility range of 1 to 10 for matching. Examples of story ductility demands obtained from a near fault record and the equivalent pulse are shown in Fig. 21 for cases of large and small ductility demands. It is observed that the important response characteristics are captured by the equivalent pulse.

The conclusion is that within the range of $0.75 < T/T_p < 3.0$ it appears to be reasonable to represent near fault ground motions by an equivalent pulse. The accuracy of such a representation is good in many cases and questionable in some. More records need to be investigated to test this hypothesis and to establish "reliable" relationships between soil type dependent pulse parameters and magnitude, distance, and fault mechanism. If this can be done, the monumental task of developing design procedures and assessing performance of structures under near fault ground motions boils down to a thorough investigation of the elastic and inelastic response of MDOF systems to a small number of pulses. A few preliminary results are summarized in the next section.

DESIGN CONSIDERATIONS FOR NEAR FAULT GROUND MOTIONS

The final goal of the work summarized here is the development of design recommendations. Such recommendations depend on the current state of knowledge and on the

design objectives, both of which are in a state of transition. The current state of knowledge on near fault ground motion effects is inadequate but growing rapidly, and design objectives are in a state of change because of the emergence of performance-based engineering. For instance, it would be inappropriate to focus only on one performance level, such as collapse prevention, because the results presented here have demonstrated that ductility demands are very sensitive not only to base shear strength but also to the story shear strength distribution over the height of the structure. On the other hand, at this time it would be inappropriate to make strong design recommendations because much more knowledge still needs to be acquired on the site dependent characteristics of near fault ground motions and on their effect on MDOF systems. Thus, only suggestions that deserve considerations in the design against near fault ground motion effects are presented here.

The results of this study indicate that it is reasonable to represent near fault ground motions by equivalent pulses, at least in the period range of $0.75 < T/T_p < 3.0$. Such pulses are defined by a pulse type, a pulse period T_p, and an effective acceleration a_{eff}. The square pulses (in the acceleration domain) shown in Fig. 7 appear to be adequate for this purpose. The type of pulse depends on the rupture mechanism and on the geologic medium between the source and the site.

Critical parameters are the pulse period T_p and a measure of pulse severity. The pulse period can be estimated with reasonable confidence from the peaks of the velocity response spectrum of the ground motion. For design purposes, the effective acceleration a_{eff} may be the most useful measure of severity, but from a ground motion perspective the effective velocity is a much more consistent parameter. It is important to note that in almost all cases the effective pulse velocity, computed as $v_{eff} = a_{eff}\ (T_p/4)$, is within 20% of the peak velocity (PGV) of the recorded near fault ground motions used in this study. It is tempting to recommend the use of the recorded peak velocity as v_{eff}, and to compute a_{eff} from this recorded parameter.

The parameters of the equivalent pulses are dependent on earthquake magnitude and closest distance to the fault, and also on the rupture mechanism. The data presented in Tables 2 and 3 provide some information on these parameters. A different approach for the determination of these parameters is proposed by Somerville, who presents preliminary relationships between pulse parameters (T_p and PGV) and seismological parameters (M_w and R) in Somerville (1998). In many cases Somerville's closed-form predictions match well with the results obtained in this study, but in some cases the match is poor. This has to be expected since the recordings come from earthquakes with different rupture mechanisms and geological source to site conditions.

Provided that the equivalent pulse parameters can be predicted as a function of M_w and R, the design process can, for a large period range, be based on pulse response studies. This does not apply to the short period range (approximately $T/T_p < 0.75$), where ground motions do not have discernable pulse characteristics. In this period range it may be appropriate to employ "standard design procedures" based on a spectrum that contains near fault modification factors. In the range of $0.75 < T/T_p < 3.0$ advantage can be taken of information of the type discussed in this paper. It should be feasible to describe the seismic demand by pulse parameters that capture the range of T_p and a_{eff} making up the seismic hazard at the site. This process needs to pay attention to expected variations in T_p and a_{eff}, and to the fact that few structures are oriented precisely in the fault-normal direction. If the latter were the case, protection against near fault ground motions would be a challenging task. This is illustrated in Fig. 22, which shows

equivalent pulse spectra for three recorded ground motions superimposed on the NEHRP soil type D spectrum. The spectral amplification would be very large over a wide range of periods.

Presuming that the hazard is given in terms of pulse type, T_p, a_{eff}, and associated pulse spectra, the task is to determine base shear demands and the shear strength distribution over the height of the structure. If the design objective is protection against damage, and elastic response is desired, the elastic spectra shown in Fig. 8 provide a good starting point for design. The base shear demand for elastic MDOF systems is related to the first mode SDOF strength demand as shown in Fig. 23. As can be seen, the MDOF/SDOF strength demand ratio is sensitive to the pulse type and the ratio T/T_p, and easily may exceed 1.0 for larger T/T_p ratios. Moreover, for T/T_p ratios greater than 1.0 the shear demand over the height of the structure is very different than for smooth 1/T-type spectra, see Fig. 10. To achieve elastic response, either the base shear strength needs to be increased further, or the story shear strength needs to be tuned to the patterns illustrated in Fig. 10. This would be a significant departure from present design practice.

A new design approach is also needed to control story ductility demands for inelastic MDOF systems. For designs that follow a standard SRSS story shear strength pattern, the story ductility demands follow the trends illustrated in Figs. 11 to 14. Since such SRSS strength designs lead to very large variations of ductility demands over the height (Figs. 11 and 12), such designs may be undesirable for protection against near fault ground motions. It can be postulated that an ideal design should produce uniform ductility demands over the height in order to utilize equally the energy dissipation capacity available in all members. The story shear strength patterns that induce uniform ductility over the height can be found through an iterative process in which story shear strengths are varied until a desirable uniform story ductility is achieved. Patterns that result in uniform target ductilities from 1 (elastic behavior) to 8 are shown in Fig. 24 for pulse P2 and $T/T_p = 2.0$. The $\mu = 1$ pattern corresponds to the elastic shear force distribution. The SRSS shear strength pattern based on a 1/T-type spectrum is also shown.

The trends are clear and consistent. For close to elastic behavior ($\mu = 1$ and 2) the story shear strength demands are high about 2/3rd up the structure, whereas for a uniform ductility of 3 or larger the demands are high at the base and decrease rapidly with height. Thus, the design shear force pattern for uniform ductility changes radically with the target ductility ratio, but the change takes place within a narrowly confined ductility range from 2 to 3.

The implications of this observation become clearer with the inspection of Fig. 25, which shows the base shear strength that is needed to limit the story ductility to a prescribed target value, for two story shear strength patterns. The solid line is for the case of the shear strength pattern causing uniform story ductility, and the dotted line is for the case of the SRSS shear force pattern. Up to a maximum story ductility of 3+ the two curves are radically different, whereas they are identical for larger ductilities. Thus, ductility control is a matter of base shear strength and story shear strength pattern, except for low strength structures ($\mu > 3.5$) in which the first story is the critical one and the story shear strength pattern no longer matters. It appears to be prudent to design a structure for a base shear strength parameter η [$\eta = (V_y/W)(g/a_{eff})$] of at least 0.25, because for smaller values of η the maximum ductility demand increases at a rapid rate. Limiting values of η for other T/T_p ratios can be obtained from the kinks in the η–μ_{max} curves

shown in Figs. 13 and 14. Once η is determined, the base shear strength parameter $\gamma = V_y/W$ can be obtained as $\gamma = \eta(a_{eff}/g)$.

A design for a minimum base shear strength as discussed in the previous paragraph should provide adequate protection against excessive ductility demands for a low performance level such as collapse prevention. It pays, however, little attention to damage control under more frequent earthquakes (smaller a_{eff}). Damage control, represented by low ductility demands, is very sensitive to the distribution of story shear strength over the height of the structure. Figure 25 delivers a clear message in this regard, as illustrated in the following example. If the design is based on a standard SRSS shear strength distribution over the height (dotted line), the maximum ductility demand remains around three for a range of η from 0.25 to 0.75, the latter corresponding to an a_{eff} that is $1/3^{rd}$ of a_{eff} for $\eta = 0.25$. Thus, significant damage has to be expected in upper stories under more frequent events (presuming that more frequent events still exhibit pulse-like near fault ground motion characteristics). However, the picture changes radically if the story shear strength distribution is tailored more towards the pattern shown in Fig. 24 for $\mu = 1$ or 2. If this is done, the maximum ductility demand for smaller a_{eff} (larger η values) decreases rapidly. This can be seen from the solid line in Fig. 25.

Thus, the two important preliminary design conclusions to be drawn are as follows. First, in order to prevent excessive ductility demands under severe earthquakes, it is important to design long period structures ($T/T_p > 1$) for a minimum strength parameter η that can be determined from kinks in the η–μ_{max} diagrams of equivalent pulses. Second, in order to provide damage control under smaller earthquakes, it is prudent to provide a story shear strength distribution over the height that is closer to the pattern for $\mu = 1$ to 2 in Fig. 24. This could be achieved through careful tuning of story shear strengths, or in the simplest case through a bilinear shear strength patterns (for instance, constant shear strength to about $2/3^{rd}$ of the structure height and linearly decreasing strength thereafter). It is a matter of economic consequences to what extent the second recommendation deserves consideration. It would be a significant departure from present practice.

CONCLUSIONS

The analytical study with near fault records and elastic and inelastic SDOF and MDOF systems has led to the following preliminary conclusions:

- SRSS modal combinations do not fully capture the traveling wave effects for elastic MDOF systems with $T/T_p > 1.0$.
- Inelastic response leads to a significant redistribution of story ductility demands that cannot be captured from an elastic spectral or dynamic analysis.
- The fault-normal component of near fault ground motions with forward directivity is very severe and has pulse-like characteristics, which in the approximate period range of $0.75 < T/T_p < 3.0$ can be represented by equivalent pulses.
- In this period range, design can be based on response characteristics of equivalent pulses, which are defined by the pulse type, the pulse period, and an effective acceleration (or velocity).

- More work needs to be done to define the site seismic hazard in terms of these pulse parameters.
- The required base shear strength for ductility control under severe earthquakes can be determined from $\eta-\mu_{max}$ curves of equivalent pulses, utilizing the aforementioned pulse parameters.
- Effective damage control for less severe near fault earthquakes necessitates a design that is based on a strength distribution over the height that is very different from the one employed in present practice.

ACKNOWLEDGEMENTS

Most of the work summarized here was carried out under a subcontract with Woodward-Clyde and was funded by the California Department of Conservation as a SMIP 1997 Data Interpretation Project. Some of the results on pulse responses were obtained in a study sponsored by Kajima Corporation as part of the CUREe/Kajima Research Program. The financial support provided by the sponsors is gratefully acknowledged. The opinions expressed in this paper are those of the authors. The contents of the paper do not necessarily represent the policy of the sponsoring agency, and no endorsement by the State Government should be assumed. The constructive collaboration of Dr. P. Somerville of Woodward-Clyde on all aspects of this research is much appreciated.

REFERENCES

Seneviratna, G.D.P.K., and Krawinkler, H., 1997. "Evaluation of Inelastic MDOF Effects for Seismic Design," *John A. Blume Earthquake Engineering Center Report No. 120*, Department of Civil Engineering, Stanford University, June 1997.

Somerville, P.G., Smith, N.F., Graves, R.W., and Abrahamson, N.A., 1997. "Modification of Empirical Strong Ground Motion Attenuation Relations to Include the Amplitude and Duration Effects of Rupture Directivity," *Seismological Research Letters*.68, 180-203.

Somerville, P.G., 1998. "Development of an Improved Ground Motion Representation for Near Fault Ground Motions," *SMIP98 Seminar on Utilization of Strong-Motion Data*, Oakland, CA, Sept. 1998.

Table 1. Designation and Properties of Recorded Fault-Normal Components

Designation	Earthquake	Station	Directivity	Magnitude	Distance
TB78tab	Tabas, 1978	Tabas	backward	7.4	1.2
LP89lgpc	Loma Prieta, 1989	Los Gatos	forward	7.0	3.5
LP89lex	Loma Prieta, 1989	Lexington	forward	7.0	6.3
CM92petr	Mendocino, 1992	Petrolia	backward	7.1	8.5
EZ92erzi	Erzincan, 1992	Erzincan	forward	6.7	2.0
LN92lucr	Landers, 1992	Lucerne	forward	7.3	1.1
NR94rrs	Nothridge, 1994	Rinaldi	forward	6.7	7.5
NR94sylm	Nothridge, 1994	Olive View	forward	6.7	6.4
KB95kobj	Kobe, 1995	JMA	forward	6.9	3.4
KB95tato	Kobe, 1995	Takatori	forward	6.9	4.3
IV40iviri	Imperial Valley, 1940	El Centro	backward	6.9	10.0
IV79ar06	Imperial Valley, 1979	Array 6	forward	6.5	1.2
IV79bond	Imperial Valley, 1979	Bond's Corn	backward	6.5	2.4
IV79melo	Imperial Valley, 1979	Meloland	forward	6.5	0.0
KB95kpi1	Kobe, 1995	Port Island	forward	6.9	6.6
LN92josh	Landers, 1992	Joshua Tree	backward	7.3	7.4
LP89corr	Loma Prieta, 1989	Corralitos	backward	7.0	3.4
MH84andd	Morgan Hill, 1984	Anderson D	forward	6.2	4.5
MH84clyd	Morgan Hill, 1984	Coyote L D	forward	6.2	0.1
MH84hall	Morgan Hill, 1984	Halls Valley	backward	6.2	2.4
NR94newh	Nothridge, 1994	Newhall	forward	6.7	7.1
NR94nord	Nothridge, 1994	Arleta	backward	6.7	9.2
NR94spva	Nothridge, 1994	Sepulveda	forward	6.7	8.9

Table 2. Equivalent Pulses for Recorded Near Fault Ground Motions (Forward Directivity)

					$\mu = 1$			$\mu = (1\text{-}10)$			$\mu = (4\text{-}10)$		
Record Name	M_w	R (km)	Pulse Type	T_p (sec)	a_{eff} (g's)	v_{eff} (cm/sec)	u_{eff} (cm)	a_{eff} (g's)	v_{eff} (cm/sec)	u_{eff} (cm)	a_{eff} (g's)	v_{eff} (cm/sec)	u_{eff} (cm)
LP89lgpc	7.0	3.5	P3	3.0	0.24	176.6	66.2	0.23	169.2	63.5	0.24	176.6	66.2
LP89lex	7.0	6.3	P2	1.0	0.71	174.1	43.5	0.81	198.7	49.7	1.04	255.1	63.8
EZ92erzi	6.7	2.0	P2	2.3	0.38	214.3	123.3	0.46	259.5	149.2	0.58	327.2	188.1
NR94rrs	6.7	7.5	P2	1.0	0.62	152.1	38.0	0.74	181.5	45.4	0.80	196.2	49.1
NR94sylm	6.7	6.4	P3	2.4	0.18	105.9	31.8	0.17	100.1	30.0	0.19	111.8	33.6
KB95kobj	6.9	3.4	P2	0.9	0.95	209.7	47.2	0.88	194.2	43.7	0.94	207.5	46.7
KB95tato	6.9	4.3	P3	2.0	0.38	186.4	46.6	0.33	161.9	40.5	0.31	152.1	38.0
IV79ar06	6.5	1.2	P2	3.4	0.13	108.4	92.1	0.13	108.4	92.1	0.16	133.4	113.4
IV79melo	6.5	0.0	P2	2.8	0.15	103.0	72.1	0.15	103.0	72.1	0.19	130.5	91.3
KB95kpi1	6.9	6.6	P2	1.8	0.28	123.6	55.6	0.24	105.9	47.7	0.27	119.2	53.6
MH84andd	6.2	4.5	P2	0.8	0.18	35.3	7.1	0.16	31.4	6.3	0.17	33.4	6.7
MH84clyd	6.2	0.1	P3	0.8	0.41	80.4	8.0	0.49	96.1	9.6	0.55	107.9	10.8
NR94newh	6.7	7.1	P2	1.3	0.39	124.3	40.4	0.34	108.4	35.2	0.40	127.5	41.4
NR94spva	6.7	8.9	P3	2.7	0.10	66.2	22.3	0.08	53.0	17.9	0.08	53.0	17.9

Table 3. Equivalent Pulses for Simulated Near Fault Ground Motions(Forward Directivity)

					$\mu = 1$			$\mu = (1\text{-}10)$			$\mu = (4\text{-}10)$		
Station	M_w	R (km)	Pulse Type	T_p (sec)	a_{eff} (g's)	v_{eff} (cm/sec)	u_{eff} (cm)	a_{eff} (g's)	v_{eff} (cm/sec)	u_{eff} (cm)	a_{eff} (g's)	v_{eff} (cm/sec)	u_{eff} (cm)
f6	6.5	3	P2	1.7	0.17	70.9	30.1	0.18	75.05	31.9	0.21	87.6	37.2
f8	6.5	3	P2	1.2	0.35	103.0	30.9	0.45	132.44	39.7	0.51	150.1	45.0
f6	6.5	5	P2	2.0	0.10	49.1	24.5	0.10	49.05	24.5	0.11	54.0	27.0
f8	6.5	5	P2	2.1	0.17	87.6	46.0	0.19	97.85	51.4	0.20	103.0	54.1
f6	6.5	10	P2	2.6	0.04	25.5	16.6	0.03	19.13	12.4	0.04	25.5	16.6
f8	6.5	10	P2	3.0	0.05	36.8	27.6	0.04	29.43	22.1	0.05	36.8	27.6
f6	7.0	3	P2	3.2	0.13	102.0	81.6	0.12	94.18	75.3	0.15	117.7	94.2
f8	7.0	3	P2	3.4	0.20	166.8	141.8	0.20	166.77	141.8	0.20	166.8	141.8
f6	7.0	5	P2	3.5	0.11	94.4	82.6	0.10	85.84	75.1	0.12	103.0	90.1
f8	7.0	5	P2	3.6	0.16	141.3	127.1	0.16	141.26	127.1	0.17	150.1	135.1
f6	7.0	10	P2	5.0	0.04	49.1	61.3	0.03	36.79	46.0	0.03	36.8	46.0
f8	7.0	10	P2	3.3	0.11	89.0	73.4	0.10	80.93	66.8	0.11	89.0	73.4
f6	7.5	3	P3	3.2	0.19	149.1	59.6	0.22	172.66	69.1	0.23	180.5	72.2
f8	7.5	3	P3	3.2	0.28	219.7	87.9	0.27	211.90	84.8	0.28	219.7	87.9
f6	7.5	5	P3	3.2	0.17	133.4	53.4	0.19	149.11	59.6	0.21	164.8	65.9
f8	7.5	5	P3	3.2	0.25	196.2	78.5	0.24	188.35	75.3	0.25	196.2	78.5
f6	7.5	10	P3	3.2	0.12	94.2	37.7	0.14	109.87	43.9	0.14	109.9	43.9
f8	7.5	10	P3	3.2	0.19	149.1	59.6	0.18	141.26	56.5	0.19	149.1	59.6

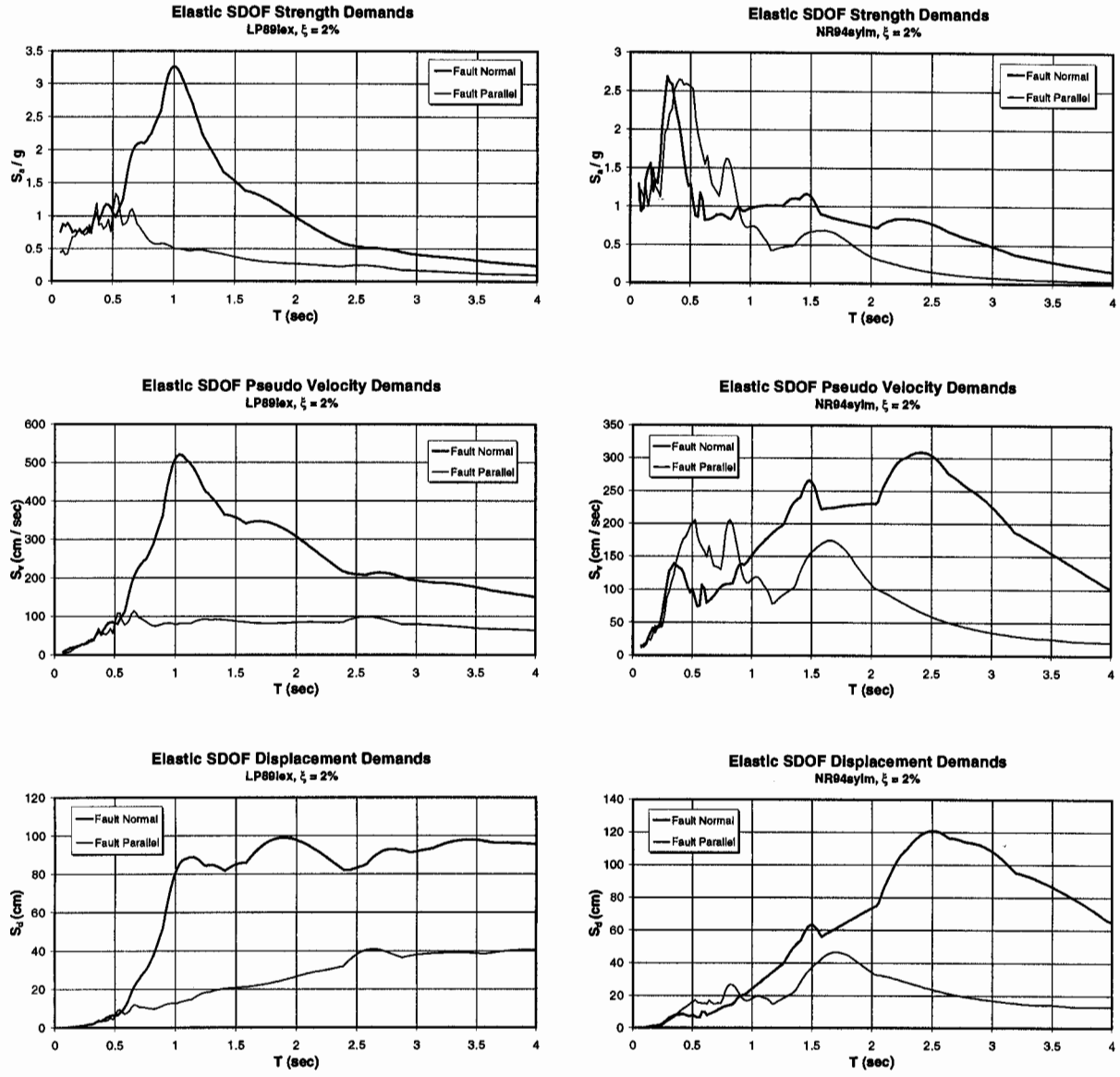

(a) Lexington Dam (LP89lex) (b) Sylmar (NR94sylm)

Figure 1. Acceleration (Elastic Strength Demand), Velocity, and Displacement Spectra of Two Recorded Ground Motions (Fault-Normal and Fault-Parallel Components)

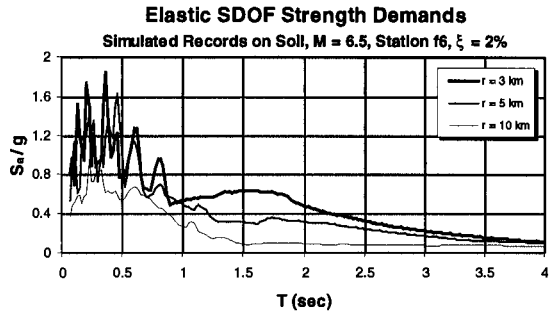

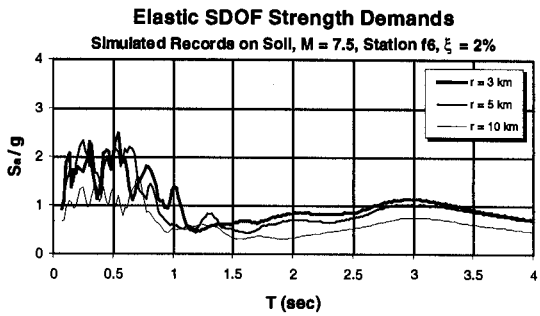

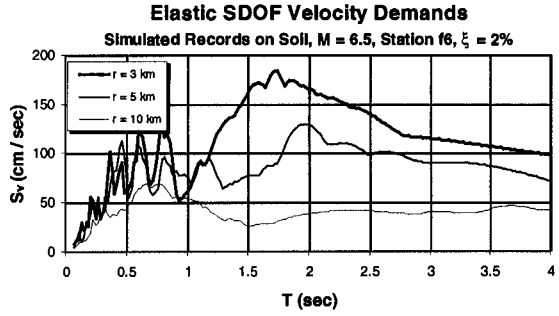

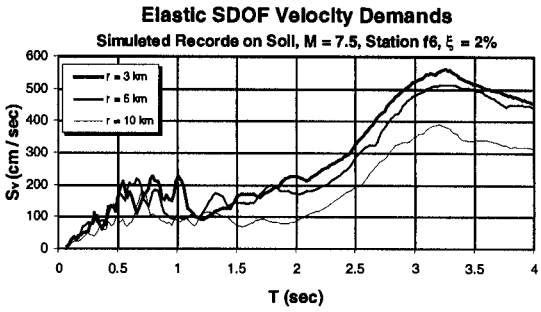

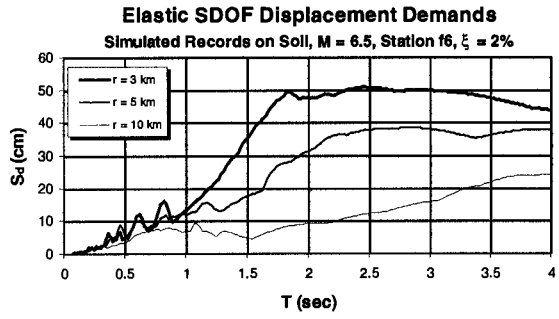

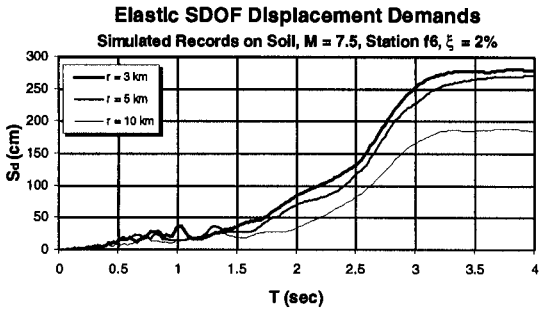

(a) Magnitude 6.5 (b) Magnitude 7.5

Figure 2. Acceleration (Elastic Strength Demand), Velocity, and Displacement Spectra of Simulated Ground Motions at Station f6 (Fault-Normal Components Only)

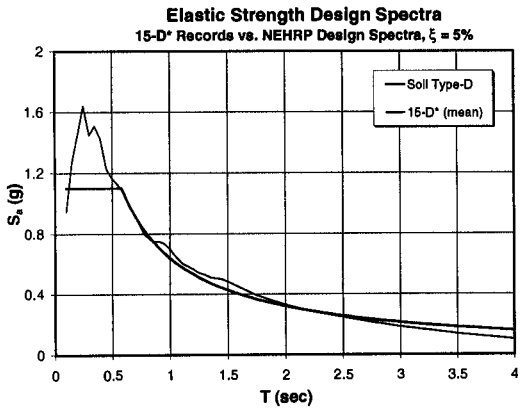

Figure 3. Mean Acceleration (Strength Demand) Spectrum of Reference Set of Records, 15-D*

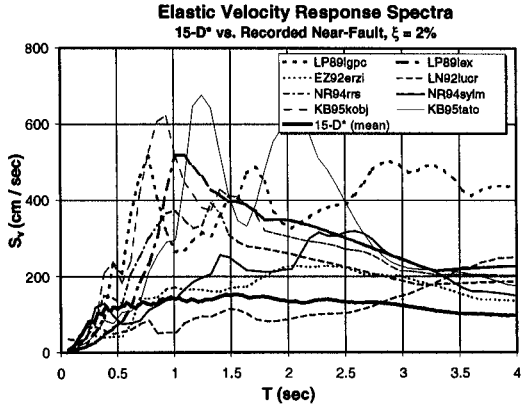

Figure 4. Velocity Response Spectra of Near Fault and Reference Ground Motions

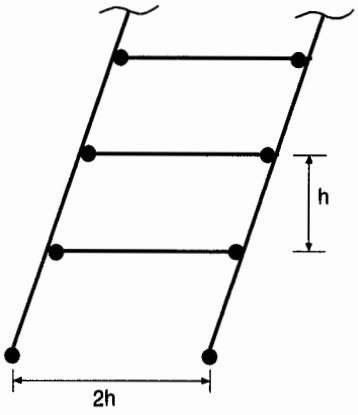

Figure 5. Global Mechanism for Generic Structure (Beam Hinge Model)

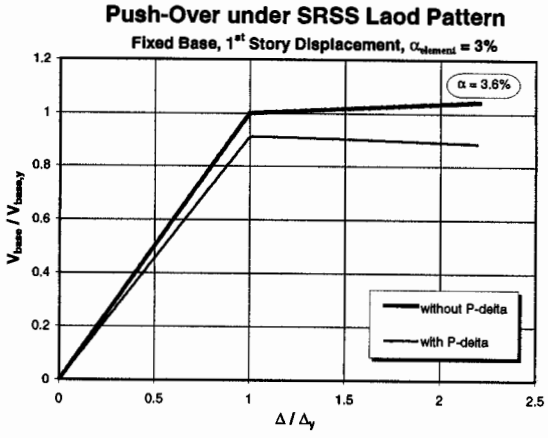

Figure 6. Pushover Response of First Story of Generic Structure with and without P-Delta

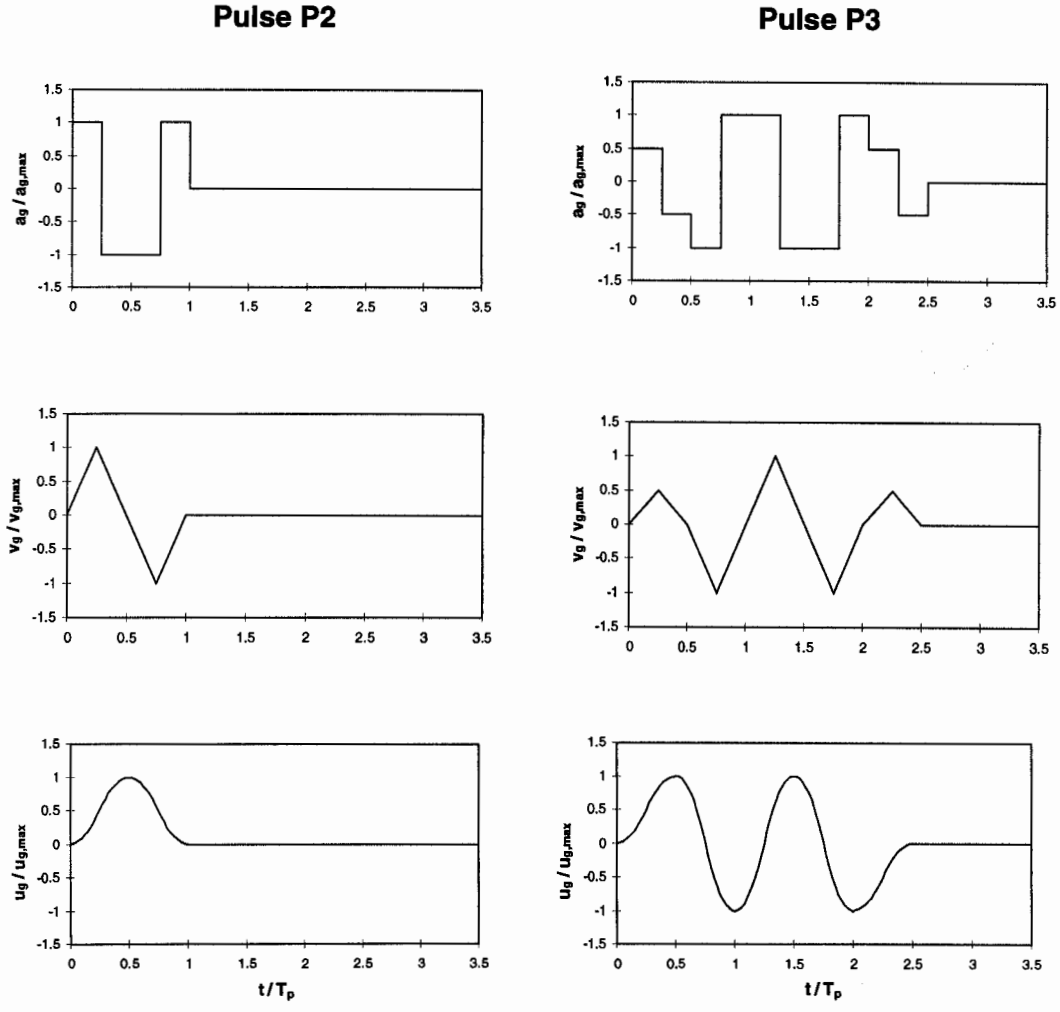

Figure 7. Acceleration, Velocity, and Displacement Time Histories of Pulses P2 and P3

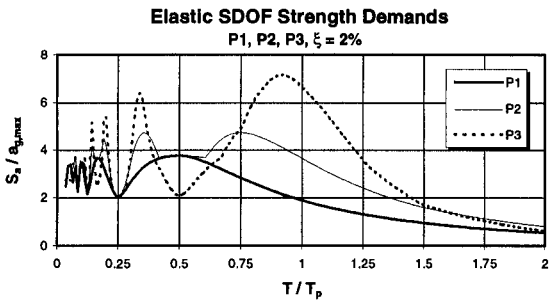

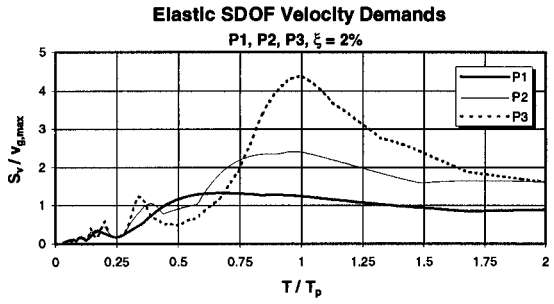

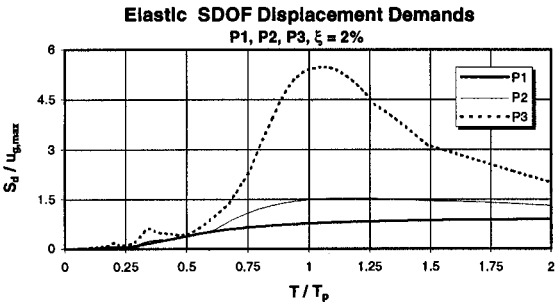

Figure 8. Elastic Strength Demand, Velocity, and Displ. Spectra for Pulses P1, P2, and P3

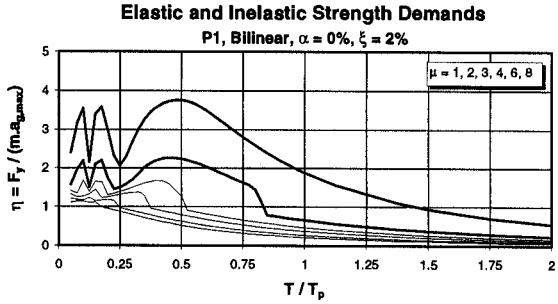

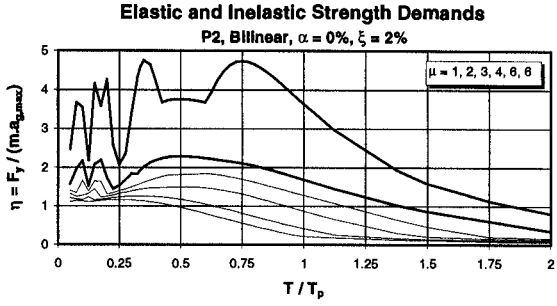

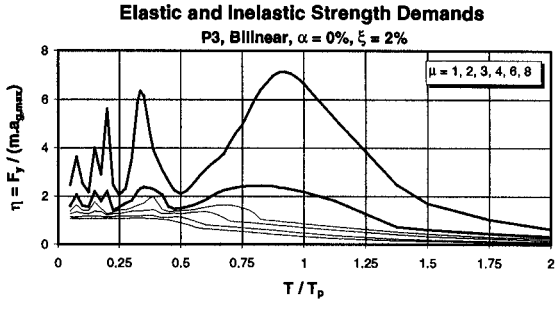

Figure 9. Elastic and Inelastic Strength Demand Spectra for Pulses P1, P2, and P3

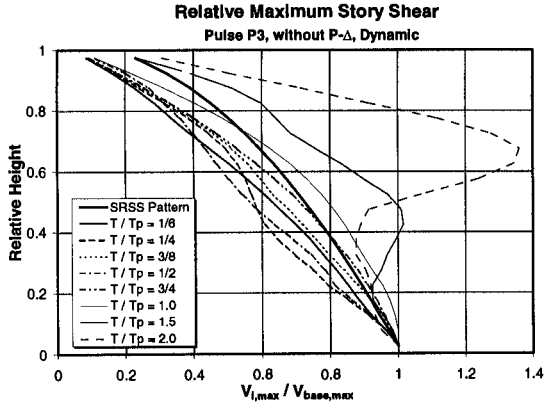

(a) From Time History Analysis

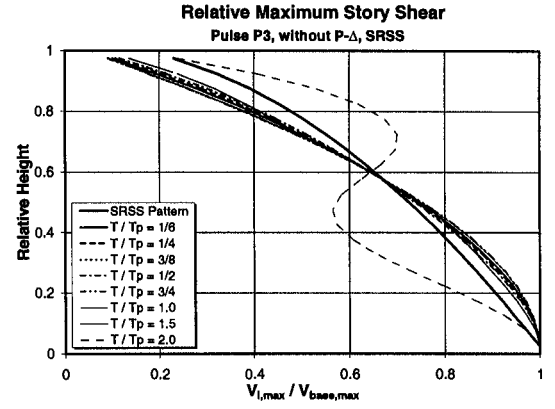

(b) From SRSS Modal Combination

Figure 10. Normalized Elastic Story Shear Demands for Pulse P3, Various Values of T/T_p

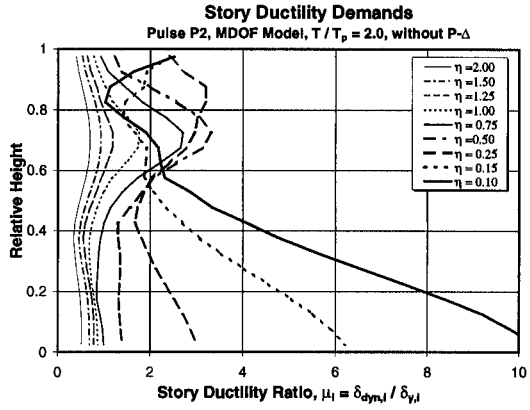

(a) $T/T_p = 2.0$

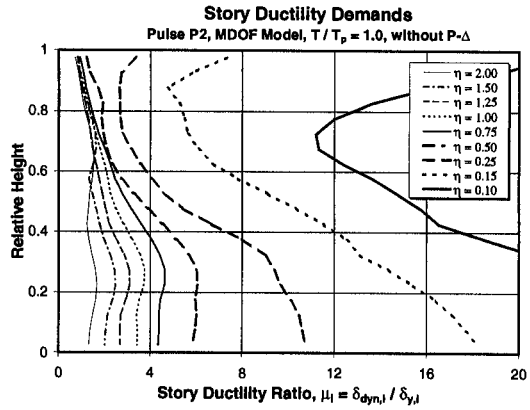

(b) $T/T_p = 1.0$

Figure 11. Story Ductility Demands for Pulse P2, Various Values of η

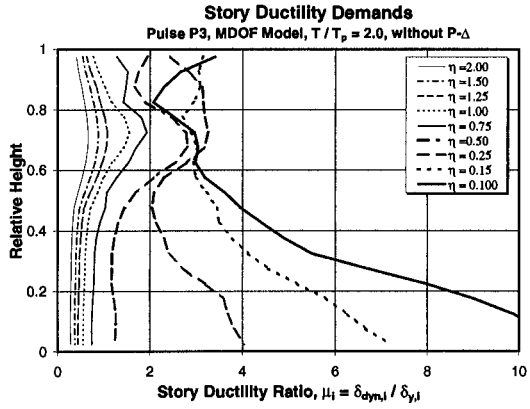

(a) $T/T_p = 2.0$

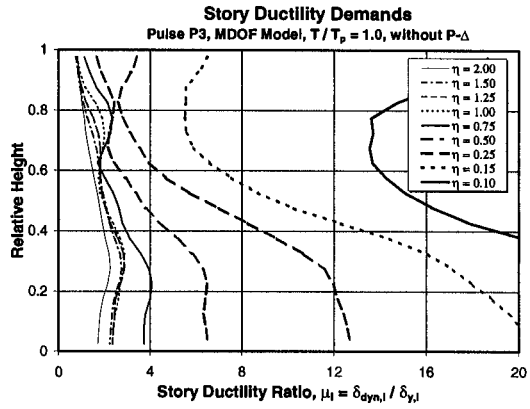

(b) $T/T_p = 1.0$

Figure 12. Story Ductility Demands for Pulse P3, Various Values of η

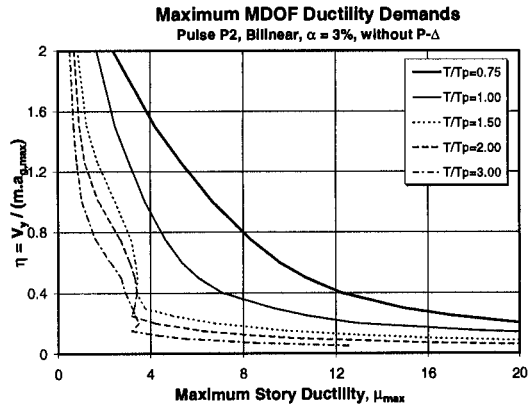

Figure 13. Base Shear Strength vs. Maximum Story Ductility Demands for Various T/T_p Values, Pulse P2

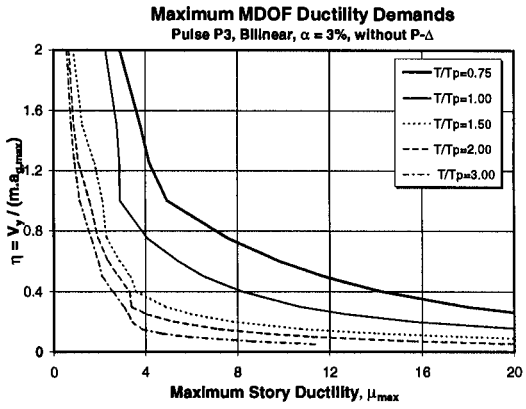

Figure 14. Base Shear Strength vs. Maximum Story Ductility Demands for Various T/T_p Values, Pulse P3

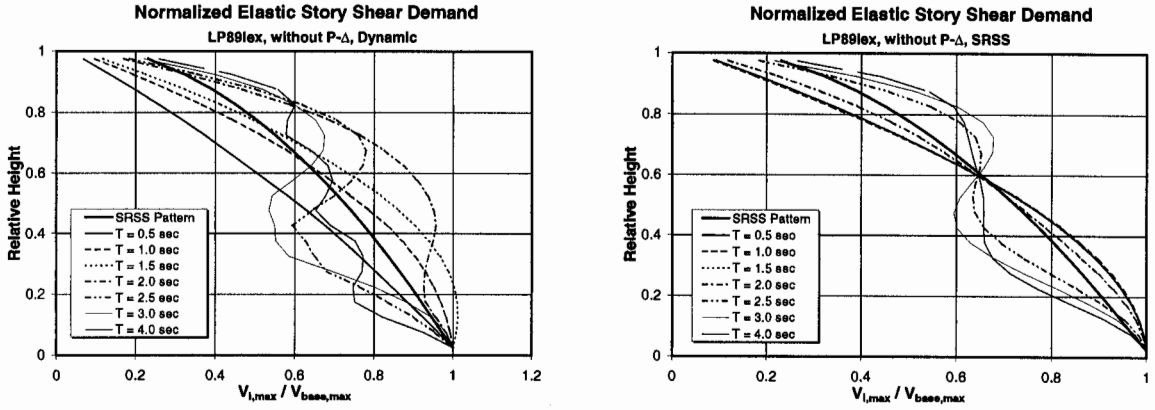

(a) From Time History Analysis (b) From SRSS Modal Combination

Figure 15. Normalized Elastic Story Shear Demands for Record LP89lex, Various Values of T

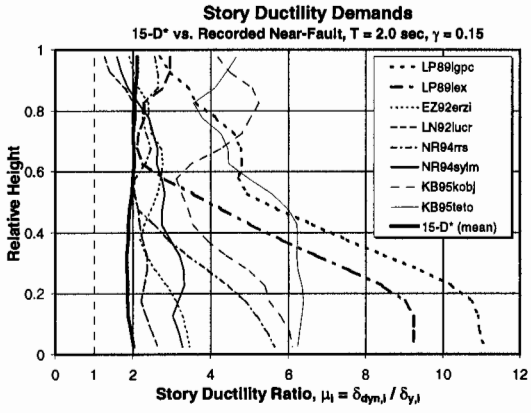

Figure 16. Story Ductility Demands for Several Near Fault Records, T = 2.0 sec., $\gamma = 0.15$

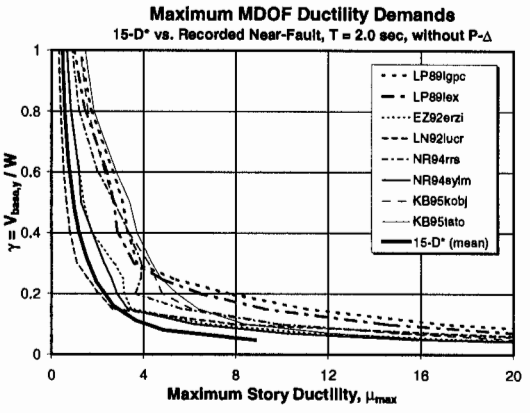

Figure 17. Base Shear Strength vs. Maximum Ductility Demand for Several Near Fault Records, T = 2.0 sec.

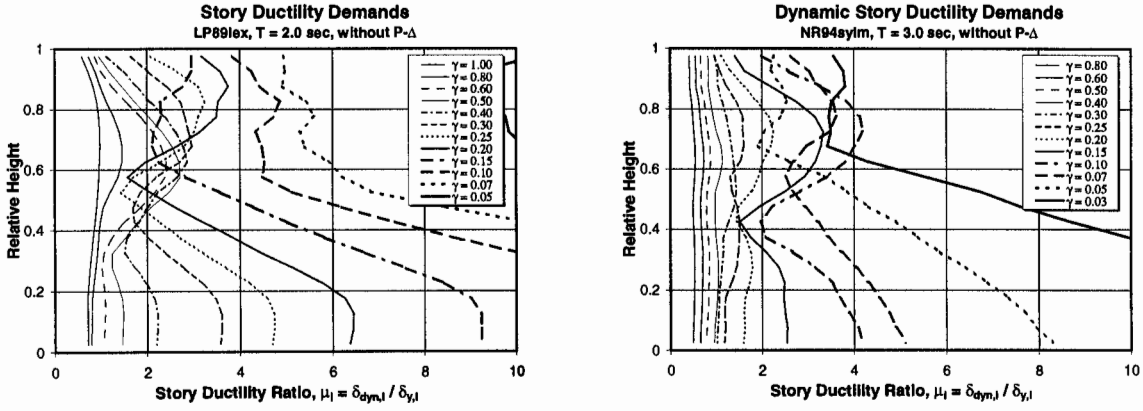

(a) Record LP89lex, T = 2.0 sec. (b) Record NR94sylm, T = 3.0 sec.

Figure 18. Dependence of Story Ductility Demands on Base Shear Strength

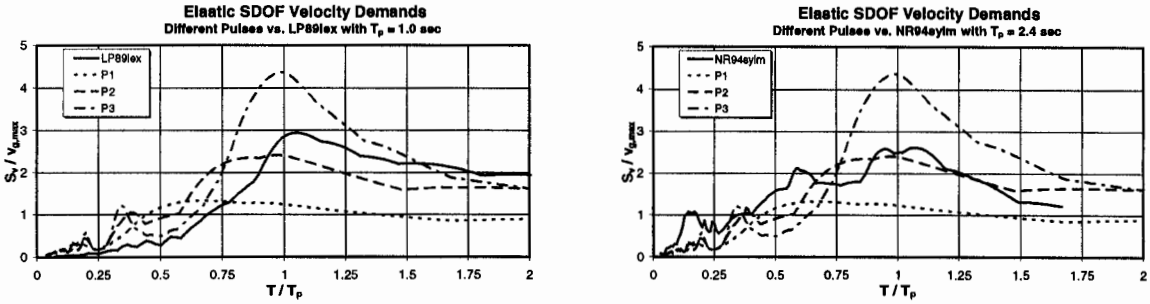

(a) Record LP89lex (b) Record NR94sylm

Figure 19. Determination of Pulse Period (and Pulse Type) from Velocity Spectra

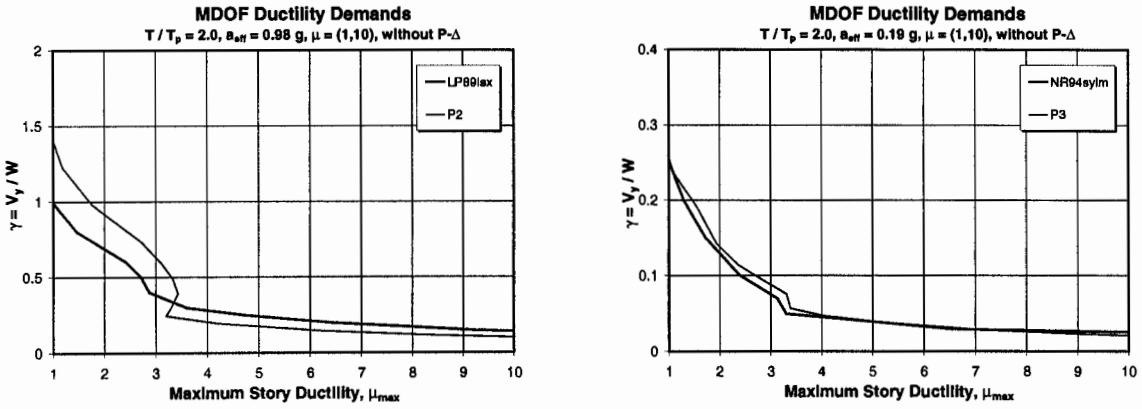

(a) Record LP89lex, $T/T_p = 2.0$ (b) Record NR94sylm, $T/T_p = 2.0$

Figure 20. Matching of γ–μ Curves for Identification of Best-Fit a_{eff}

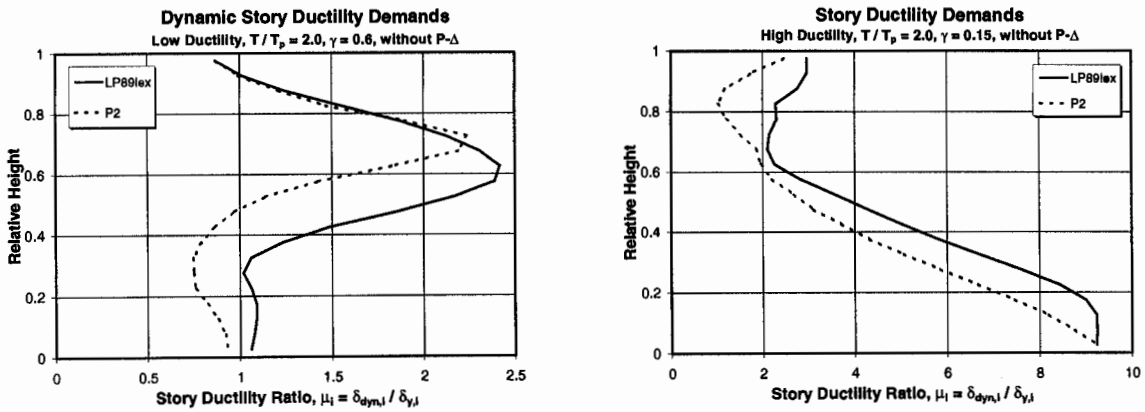

(a) High Strength, Low Ductility (b) Low Strength, High Ductility

Figure 21. Story Ductility Demands Obtained from a Near Fault Record and its Equivalent Pulse

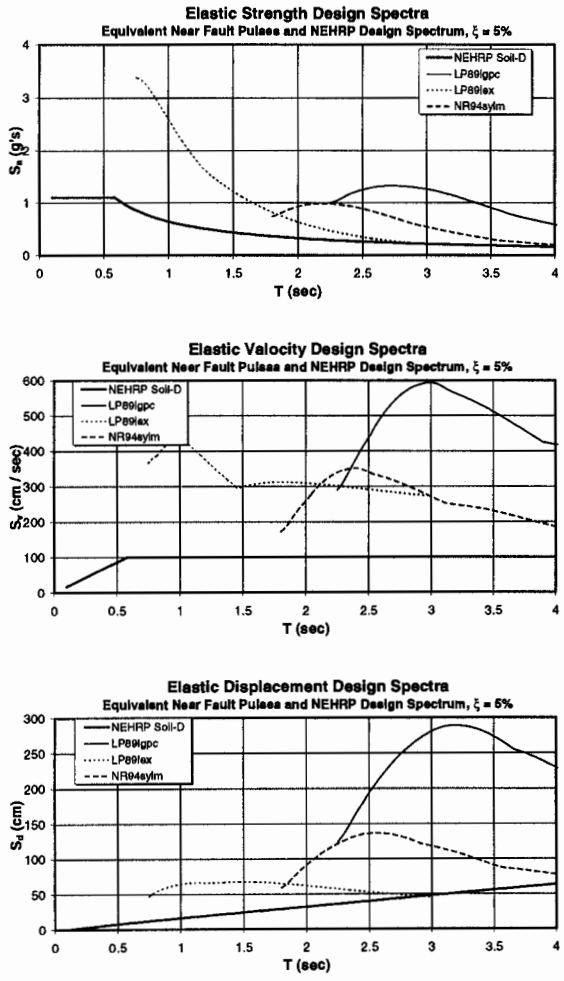

Figure 22. Examples of Near Fault Equivalent Pulse Spectra Superimposed on NEHRP Design Spectra

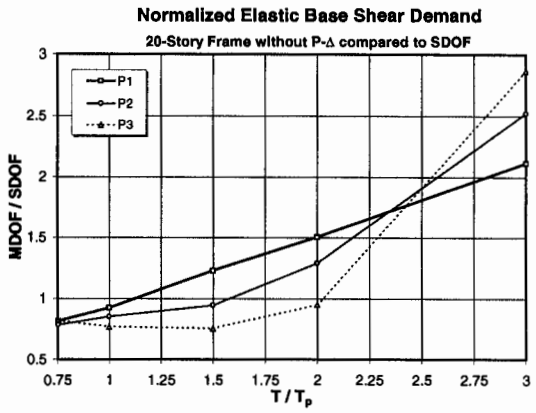

Figure 23. Ratio of MDOF Base Shear to SDOF Strength Demand for Elastic Systems

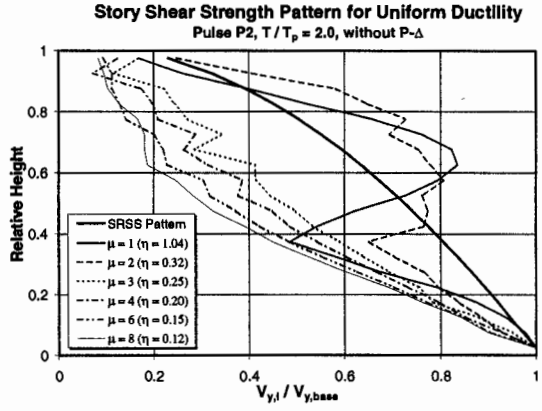

Figure 24. Story Shear Strength Patterns for Target "Uniform Ductilities" Over Height; Pulse P2, $T/T_p = 2.0$

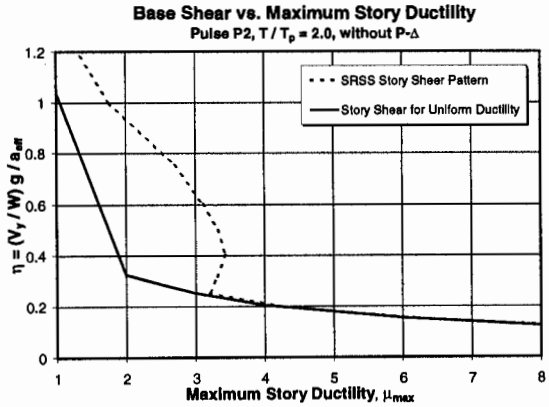

Figure 25. Base Shear Demands for Specific Target Ductilities; SRSS and "Uniform Ductility" Shear Strength Patterns; Pulse P2, $T/T_p = 2.0$